Charge renormalization in nominally apolar colloidal dispersions

Daniel J. Evans, Andrew D. Hollingsworth, and David G. Grier[*]

Department of Physics and Center for Soft Matter Research, New York University, New York, New York 10003, USA

We present high-resolution measurements of the pair interactions between dielectric spheres dispersed in a fluid medium with a low dielectric constant. Despite the absence of charge control agents or added organic salts, these measurements reveal strong and long-ranged repulsions consistent with substantial charges on the particles whose interactions are screened by trace concentrations of mobile ions in solution. The dependence of the estimated charge on the particles' radii is consistent with charge renormalization theory and, thus, offers insights into the charging mechanism in this interesting class of model systems. The measurement technique, based on optical-tweezer manipulation and artifact-free particle tracking, makes use of optimal statistical methods to reduce measurement errors to the femtonewton frontier while covering an extremely wide range of interaction energies.

The linearized Poisson-Boltzmann model for colloidal electrostatic interactions predicts that like-charged spheres dispersed in aqueous electrolytes interact through a screened-Coulomb repulsion [1]. This model agrees well with direct measurements of the interactions between pairs of charged colloidal spheres dispersed in water at a low ionic strength [2,3]. Surface charges develop on these particles through dissociation of ionizable groups [4] and are screened by atomic-scale counterions in solution. Agreement with the predicted screened-Coulomb form is obtained even for particles that carry charges so large that the approximations underlying the linearized Poisson-Boltzmann model no longer apply. The effective charges parameterizing these interactions then are consistent with charge renormalization theory [3,5,6]. Here, we show that linearized Poisson-Boltzmann theory also describes the interactions between nominally uncharged acrylic spheres dispersed in a nominally apolar medium and that the effective charges on these particles are large enough to be described by charge renormalization theory.

The particles used for this study are dispersion-polymerized poly(methyl methacrylate) (PMMA) spheres [7,8] suspended in a mixture of cyclohexyl bromide (CXB) and dodecane. The particles have a density of 1.19 g mL^{-1} and a refractive index of $n_p = 1.492$ at a wavelength of $\lambda = 532$ nm. Adding 16% dodecane, by weight, to CXB yields a density-matching medium with an estimated dielectric constant [9] of $\epsilon = 5.9$ and a refractive index of $n_m = 1.4745$. The refractive index contrast ($n_p - n_m = 0.0175$) is large enough that the particles can be imaged in a conventional bright-field microscope without fluorescent labeling and can be trapped with conventional optical tweezers. All quantities were measured at 20°C.

The PMMA particles have nonionogenic surfaces that are sterically stabilized with poly(12-hydroxystearic acid) (PHS) [10]. When dispersed in an apolar index-matching medium, similar particles have been shown to act as a model hard-sphere system [11] characterized by contact repulsions but no longer-ranged interactions. These spheres can be rendered neutrally buoyant through the addition of density-matching cosolvents

such as tetrachloroethylene without affecting their long-ranged interactions [12]. When dispersed in CXB, however, these particles can display extremely long-ranged repulsions that are strong enough to stabilize colloidal crystals at volume fractions below 10^{-3} [13]. These repulsions arise from positive surface charges that are believed to be built up by association of positively charged species in solution with the particles' surfaces, or with the PHS layer covering the surfaces, or both. These positive species, in turn, are believed to arise from hydrolysis of CXB leading to dehydrobromination. The resulting hydrogen bromide then dissociates slightly to produce protons that contribute to the spheres' charges and bromide ions that remain in solution [13,14]. The presence of a tertiary amine catalyst used to attach the graft copolymer stabilizer layer recently has been implicated in the charging process [15].

The impurity content of "as received" CXB (Sigma Aldrich; ⩾98%) depends on its age and storage conditions. Prior to using the CXB, we pass it though an activated alumina column to remove polar and acidic molecules such as H_2O and HBr [16]. The measured conductivity subsequently decreases by one or two orders of magnitude. No effort was made to rigorously exclude moisture from the CXB aside from padding the storage bottles with dry nitrogen. An "intrinsic" conductivity of $\mathcal{O}\{10^{-9}\}$ S m^{-1} is typically observed in the purified CXB [13–15], which remains reasonably constant for several weeks. Hydrolysis reactions, stemming from the presence of trace amounts of water, are believed to produce hydrogen bromide via elimination reactions and nucleophilic substitution [17,18]. As a result, the conductivity will slowly rise with time. Kinetic studies of the hydrolysis of alicyclic bromide compounds, including CXB, have been reported using a conductivity method [19].

The degree to which HBr can dissociate in solution is controlled by the Bjerrum length,

$$\lambda_B = \frac{e^2}{4\pi \epsilon \epsilon_0 k_B T},\qquad(1)$$

at which distance the Coulomb interaction between two monovalent ions is equal in magnitude to the thermal energy scale, $k_B T$, at absolute temperature T. Here, ϵ_0 is the

---

[*]david.grier@nyu.edu

vacuum permittivity, k_B is Boltzmann's constant, and e is the elementary charge. The Bjerrum length in water at room temperature is 0.7 nm. Solvation of ions by water molecules therefore yields stable charge separation [20]. Dodecane's Bjerrum length of 28.3 nm, by contrast, is much larger than the molecular scale. Ion solvation is only possible in such an environment if micelles or similar large-scale structures participate in maintaining charge separation [21–23]. The Bjerrum length of the CXB-dodecane mixture is 9.6 nm, which limits the concentration of mobile ions but does not preclude their existence [24,25].

The presence of a low concentration of solvated ions in the CXB-dodecane mixture is suggested by the solution's conductivity, which is measured to be $\sigma = 2.6 \times 10^{-9}$ S m^{-1} using a Scientifica model 627 conductivity meter. This is related to the concentration, n, of dissolved ions by $\sigma = \Lambda_0 n$, where Λ_0 is the limiting molar conductance of the ions in the CXB-dodecane mixture. Assuming that ionic currents are carried by dissociated HBr, we can estimate Λ_0 from the previously measured value, $\Lambda_b = 11.4$ cm^2 S mol^{-1}, for HBr in 2-butanol ($\epsilon = 16.6$) [26] using the Walden product $\Lambda_0 \eta_0 = \Lambda_b \eta_b$. Here, $\eta_0 = (1.945 \pm 0.005)$ mPa s is the viscosity of the CXB-dodecane solution, as measured by capillary viscometry, and $\eta_b = 3.501$ mPa s is the corresponding value for 2-butanol [27]. From this, we obtain $\Lambda_0 = 20.5$ cm^2 S mol^{-1} and a total concentration of monovalent ions of $n = (1.27 \pm 0.05) \times 10^{-9}\,M$. In a conventional electrolyte, dissolved ions contribute to the Debye-Hückel screening length, κ^{-1}, given by

$$\kappa^2 = 4\pi \lambda_B n N_A, \qquad (2)$$

where N_A is Avogadro's number. For the bulk CXB-dodecane solution in the absence of spheres, we obtain $\kappa_b^{-1} = (3.4 \pm 0.1)\,\mu$m.

The nominally neutral PMMA spheres acquire charges when dispersed in this solvent. The presence and positive sign of these charges are confirmed through electrophoresis performed with a Malvern Zetasizer Nano ZS with a universal dip cell (ZEN1002). Neither the solvation of the ions nor the presence of charges on the spheres relies on the addition of charge-stabilizing agents.

One possible origin for the spheres' positive charge is an ion-dipole association between cations in solution and the polar carbonyl groups of the PHS stabilizer layer, including the intended diester linkage between the epoxide-functionalized PHS-g-PMMA stabilizer and surface acid groups. This idea was proposed originally to explain the apparent surface charge behavior of similar colloidal particles suspended in dodecane with added salt [28,29]. Recently, an alternative mechanism has been proposed [15] in which protons associate with tertiary amine-terminated surface groups resulting from a competing chemical reaction between the catalyst used to couple the stabilizer and the carboxylic acid groups present on the particle surface. The carbonyl groups' dipole moments are four times greater than the amine groups', however [30,31]. If we account for the entire PHS molecule at an average surface coverage per soluble moiety of 3.5 nm^2 [32] and use 1740 for the average PHS molecular weight [7], we estimate that there are between 10 and 100 more carbonyl groups than amine groups available for proton binding. It is likely that both reactions take place during the so-called stabilizer "locking stage" using

dimethylethanolamine. Regardless of the type of dipole at or near the particle surface, the particle charging mechanism would be the same.

Here, we report on blinking-optical-tweezer measurements [2,3,33,34] of the colloidal spheres' interactions in this unusual electrolyte. These measurements yield estimates of the spheres' charges and the electrolyte's screening length. Our analysis uses adaptive kernel density estimators [35] to make optimal use of unevenly sampled trajectory data, thereby achieving femtonewton force resolution over a wide range of particle separations. The results of these measurements are consistent with screened-Coulomb repulsions between like-charged spheres in quantitative agreement with predictions of the linearized Poisson-Boltzmann model. The spheres' effective charges are found to scale linearly with their radii in a manner consistent with charge renormalization theory. The Debye-Hückel screening length obtained from these measurements is significantly longer than the value inferred from the solution's bulk conductivity yet shorter than the values estimated from the lattice constants of colloidal crystals formed from similar particles [14].

Our sample cell consists of a rectangular borosilicate capillary tube (Vitrocom 5010) whose interior thickness is 100 μm, which is attached to a standard microscope slide with optical adhesive (Norland Type 68). The capillary tube is shielded with foil to protect the CXB from ultraviolet photolysis during the curing process. Three-quarters of the chamber is filled with a suspension of PMMA particles in a density-matching medium at an initial volume fraction of $\phi \sim 10^{-3}$. The remainder of the channel is filled with deionized water. Positively charged particles rapidly deposit onto the glass channel's inner surfaces to form a stabilizing layer that prevents further deposition. The remaining particles remain suspended at a volume fraction of about 10^{-5} for at least a month. No more than 50 spheres are immobilized in the field of view. These are few enough and far enough from the focal plane not to interfere with trapping or tracking the pairs of spheres used for interaction measurements.

The equilibrated sample is mounted for observation on the stage of an inverted optical microscope (Zeiss Axiovert T100 2TV) outfitted with an oil-immersion objective lens (Zeiss Plan Apo; numerical aperture, 1.4) with a magnification of 100× for particles with radii smaller than $a_p = 1.5$ μm and 63× for larger particles. The objective lens is used to project a pair of holographic optical tweezers into the sample [36,37] at a vacuum wavelength of 532 nm (Coherent Verdi V-5). The laser beam's wave fronts are appropriately shaped by a liquid-crystal spatial light modulator (Hamamatsu PPM X8267).

As shown schematically in Fig. 1(a), two optical traps are used to move a pair of spheres to the midplane of the sample cell at a specified center-to-center separation r. Once positioned, the particles are released, and their motions are recorded at 1500 frames/s with a digital high-speed video camera. The camera's exposure time, 0.6 ms, is short enough to avoid artifacts due to motion blurring [38,39]. Figure 1(b) shows a detail of a typical video frame of two 2.3-μm-diameter spheres obtained 3 ms after the particles were released. The spheres' in-plane positions are determined to within 10 nm in each snapshot using standard methods of digital video microscopy [33]. The circles overlaid on the image in Fig. 1(b)
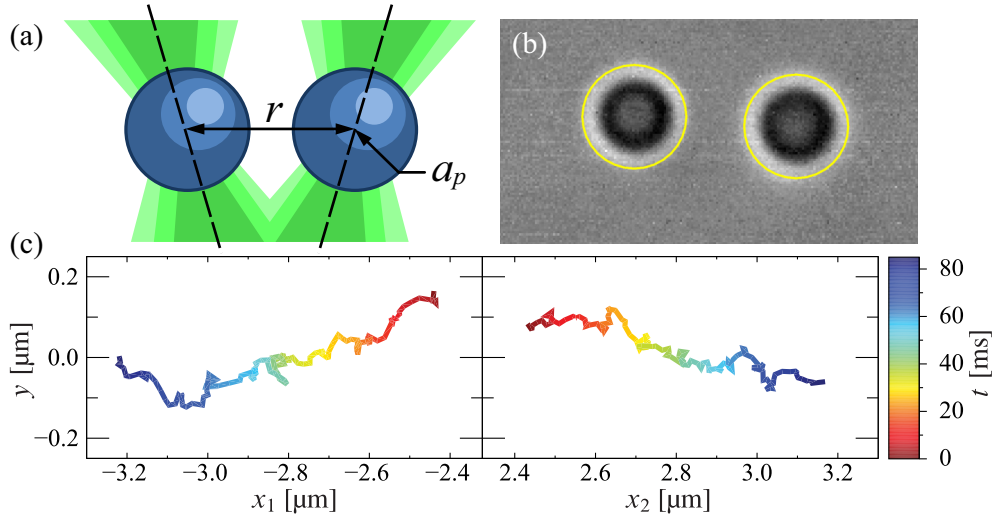
FIG. 1. (a) Schematic of a two-particle blinking optical trapping experiment with the traps on. (b) Typical bright-field image of 2.3-μm-diameter PMMA spheres in CXB-dodecane overlain with circles marking the measured sphere positions. (c) Single-blink trajectory of 2.3-μm spheres with an initial particle separation of 4.8 μm. The particles move 1.6 μm within the 86-ms blink period.

are centered on the particles' positions. Care was taken in these measurements [40] to avoid tracking artifacts due to overlap of the spheres' diffraction patterns [41]. Location data from consecutive frames are linked into trajectories, as shown in Fig. 1(c). The complete data set then consists of a set of trajectories obtained over a range of starting separations.

Repeatedly trapping and releasing pairs of spheres builds statistics for the particles' trajectories from which we can extract estimates for the interparticle interaction [2,34]. Keeping the particles more than 40 μm from the nearest glass surface minimizes any influence of hydrodynamic coupling to the walls [42–44]. The traps are extinguished for 100 ms in each 700-ms blink cycle, these times being selected to ensure that the particles are reliably recaptured at the end of each cycle. These intervals also are short enough that tracking errors due to the spheres' out-of-plane diffusion may be ignored. The particles move freely while the traps are off, and the camera is triggered to record a sequence of 130 frames over a period of 86 ms. Missing 10 ms at the beginning and 4 ms at the end of each blink ensures that the traps are fully extinguished during data acquisition and gives the system some time to relax from any light-induced perturbations. The data in Fig. 1(c) were recorded during a single blink.

Particles' trajectories encode information about their interactions. Assuming that the medium is isotropic and that its viscosity is high enough that the particles' motions are overdamped, the particles both diffuse under the influence of random thermal forces and drift under the influence of their mutual interaction. If we project the particles' motions into the direction connecting their centers, they are as likely to diffuse together as they are to diffuse apart. In that case, an ensemble average of the projected relative velocity yields the center-to-center drift velocity, $v(r)$, which is related to the interparticle force, $F(r)$, by

$$v(r) = \mu(r)\, F(r), \qquad (3)$$

where $\mu(r)$ is the pair mobility for relative motion along $\hat{\mathbf{r}}$ at separation r. Provided that $\mu(r)$ is known, measurements of $\mathbf{v}(\mathbf{r})$ yield estimates for the interparticle force, $F(r)$.

As pointed out in Ref. [34], the particles' relative diffusivity $D(r)$ along the axial direction also depends on their relative axial mobility through the Einstein relation

$$D(r) = \mu(r)\, k_B T. \qquad (4)$$

The diffusivity can be obtained from the same trajectory data by computing the ensemble average of the fluctuations in the particles' relative velocity. Combining Eqs. (3) and (4) therefore yields an estimate of the interparticle force,

$$F(r) = k_B T\, \frac{v(r)}{D(r)}, \qquad (5)$$

which can be computed self-consistently from a set of trajectory data [21,34,45,46].

The pair separation, $\mathbf{r}(t)$, is recorded at even time intervals, τ. The resulting time series from a particular blink may be represented as a discrete set $\{\mathbf{r}_j\}$ of separations measured at time $t_j = j\tau$. The relative velocity, $\mathbf{v}_j$, at time t_j may be estimated from the change in position over n of these time intervals and may be associated with the midpoint separation $\mathbf{R}_{j,n} = (\mathbf{r}_{j+n} + \mathbf{r}_j)/2$. The relative drift velocity then can be obtained by projecting $\mathbf{v}_{j,n}$ onto the direction of the midpoint separation:

$$v_{j,n} = \frac{\mathbf{r}_{j+n} - \mathbf{r}_j}{n\tau} \cdot \hat{\mathbf{R}}_{j,n}. \qquad (6)$$

This projection suppresses projection errors that would result in the appearance of a fictive outward drift [2,3,33] due to diffusion in more than one dimension. Values of $v_{j,n}$ and $R_{j,n}$ are used to estimate $F(r)$. Assuming that no relevant control parameters vary over the course of a measurement, data from multiple blinks obtained over a range of starting separations can be consolidated into a single data set for analysis.

An outstanding challenge in this technique has been to make the most efficient use possible of measured trajectory data.

Sampling particle separations uniformly is difficult because particles move most rapidly at small separations where they interact most strongly. Measurements in this region benefit from larger numbers of blinks starting from small separations. Conversely, probing weak interactions at large separations poses challenges because particles tend not to move very far once they are released. Measurements in this region benefit from sequences of blinks that cover a range of separations evenly. Unfortunately, the information required to plan a sequence of starting conditions for uniform statistical sampling is available only after the measurement is completed and the interaction is known. To address this problem, we use adaptive kernel density estimators [35] to make optimal use of unevenly sampled data.

The estimate for the relative velocity at separation r based on an N-measurement data set is

$$\bar{v}_n(r) = \frac{1}{\rho_n(r)} \frac{1}{N-n} \sum_{j=1}^{N-n} v_{j,n} \delta_{\sigma_j}(r - R_{j,n}), \qquad (7)$$

where the kernel, $\delta_\sigma(r)$, is a smoothing function whose width, σ, is computed self-consistently from the local density of measurements [35],

$$\bar{\rho}_n(r) = \frac{1}{N-n} \sum_{j=1}^{N-n} \delta_{\sigma_j}(r - r_{j,n}). \qquad (8)$$

The typical results presented in Fig. 2 were obtained with the Epanechnikov kernel; quantitatively equivalent results are obtained with other choices, including a Gaussian kernel. Figure 2(a) shows the density of measurements at unit time interval, $n = 1$, for a typical blinking-tweezer measurement. These data represent results from $N = 1000$ single-blink trajectories obtained with a pair of 2.3-μm-diameter spheres acquired over a period of 10 min. Nonuniformity in the density estimate shown in Fig. 2(a) reflects the fact that the like-charged spheres spend comparatively little time in close proximity. Figure 2(b) shows the corresponding result for the drift velocity for that particular pair of spheres. Fluctuations in the separation-dependent relative velocity are accentuated by the logarithmic scale in Fig. 2(b), with statistical error estimates indicated by the surrounding shaded region.

We obtain the separation-dependent relative diffusion coefficient from estimates of the velocity fluctuations, which are computed from the same trajectory data as

$$\Delta \bar{v}_n^2(r) = \frac{1}{\rho_n(r)} \frac{1}{N-n} \sum_{j=1}^{N-n} v_{j,n}^2 \delta_{\sigma_j}(r - r_{j,n}) - \bar{v}_n^2(r). \quad (9)$$

These mean-square fluctuations are then related to the pair diffusion coefficient through the Einstein-Smoluchowski relation,

$$\Delta \bar{v}_n^2(r) = \frac{2}{n\tau} D(r) + \frac{2}{n^2\tau^2} \epsilon^2(r), \qquad (10)$$

taking into account the measurement error in the pair separation, $\epsilon(r)$ [33,38,39], which may depend on the separation. Assuming that $\epsilon(r)$ has zero mean, these errors should not affect the estimate for the relative velocity. Because measurement errors should not depend on the interval n

between samples, we may estimate the separation-dependent relative diffusion coefficient from any pair of estimators as

$$\bar{D}(r) = \tau \frac{\Delta \bar{v}_{n'}^2(r) n'^2 - \Delta \bar{v}_n^2(r) n^2}{2(n' - n)}. \qquad (11)$$

In computing $\bar{v}_n^2(r)$ and $\Delta \bar{v}_n^2(r)$ over intervals $n > 1$, we use overlapping samples from the trajectory data set, also known as greedy sampling [47]. This should not affect estimates for $v(r)$ or $D(r)$ provided that the trajectories may be treated as Markov processes. This, in turn, requires that the time interval $n\tau$ be short enough that the particles' relative motion cause negligibly small changes in the force and mobility associated with separation r. Whether or not this condition has been met can be assessed after a measurement is complete.

Figure 2(c) shows the estimate of $D(r)$ obtained with $n = 1$ and $n' = 2$. The solid curve in Fig. 2(c) is a fit to the leading-order prediction [48–50]

$$D(r) = 2D_0 \left[1 - \frac{3}{2} \frac{a_p}{r} + \mathcal{O}\left\{ \left(\frac{a_p}{r} \right)^3 \right\} \right] \qquad (12)$$

for the single-sphere diffusion coefficient, D_0. The fit value, $D_0 = (0.104 \pm 0.004) \, \mu\text{m}^2 \, \text{s}^{-1}$, is consistent with the Stokes-Einstein value, $D_0 = k_B T/(6\pi \eta_0 a_p) = (0.096 \pm 0.005) \, \mu\text{m}^2 \, \text{s}^{-1}$. In that sense, the curve in Fig. 2(c) may be considered to be a no-free-parameter comparison with theory, rather than the result of a fit. The dashed line in Fig. 2(c) indicates the asymptotic asymptotic diffusion coefficient, $2D_0$.

Combining the estimate for the relative velocity, $\bar{v}(r)$, with the estimate for the relative pair diffusivity, $\bar{D}(r)$, yields the estimate for the interparticle force, $\bar{F}(r)$, plotted in Fig. 2(d). As is typical for all of the particle pairs measured, these spheres repel each other with a force that falls off with increasing separation.

At least as a point of departure, it seems reasonable to compare these results with the predictions of the linearized Poisson-Boltzmann theory for colloidal electrostatic interactions in simple electrolytes. Any discrepancies then would cast light on ways in which the CXB-dodecane system departs from this idealized model and on unusual charging mechanisms for the spheres. The pair interaction between identical spheres then can be described as a screened-Coulomb repulsion [1],

$$U_{\text{sc}}(r) = k_B T \, Z^{*2} \lambda_B \left(\frac{e^{\kappa a_p}}{1 + \kappa a_p} \right)^2 \frac{e^{-\kappa r}}{r}, \qquad (13)$$

where Z^* is the effective charge number on each sphere. In conventional aqueous electrolytes, the squared term in Eq. (13) accounts for the exclusion of simple ions from the spheres' interior. The solid curve in Fig. 2(d) is a two-parameter fit to

$$F_{\text{sc}}(r) = \left(\kappa + \frac{1}{r} \right) U_{\text{sc}}(r) \qquad (14)$$

for the spheres' effective charge number, $Z^* = 687 \pm 20$, and the electrolyte's screening length in the presence of spheres, $\kappa_s^{-1} = (6.2 \pm 0.1) \, \mu\text{m}$. Consistent values for the effective charge have been inferred from the pair correlation function of similar many-sphere dispersions [51].
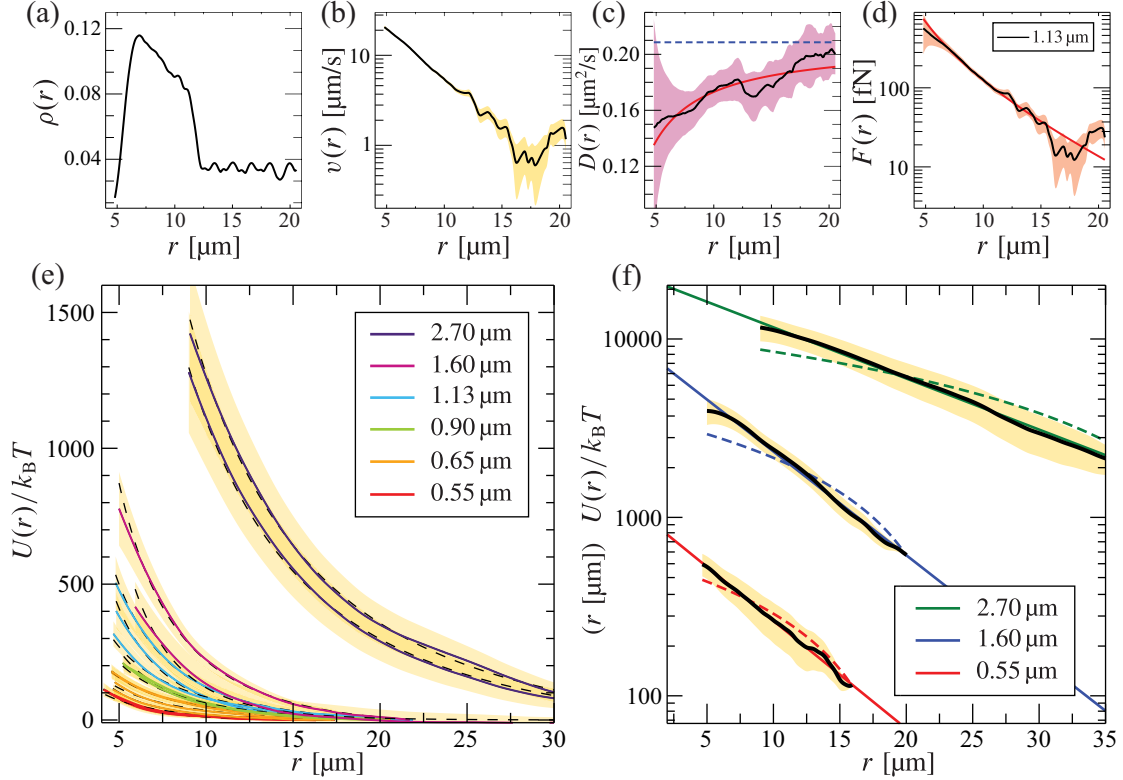
FIG. 2. Kernel density estimates of (a) the probability distribution function $\rho(r)$, (b) the velocity $v(r)$, (c) the diffusivity $D(r)$, and (d) the force $F(r)$, all as functions of particle separation r for 2.3-μm-diameter spheres. (e) Pair potentials $U(r)$ in units of the thermal energy scale for spheres of various sizes obtained by numerically integrating measured pair forces. (f) Selected data from (e) replotted to emphasize the screened-Coulomb form. Dashed curves are best fits to the pure Coulomb repulsion. Shaded regions are uncertainties for the relevant quantities.

The screening length estimated from the spheres' interactions is significantly larger than the bulk value, κ_b^{-1}, estimated from the solvent's conductivity. The ratio of the respective ionic strengths is $n_s/n_b = (\kappa_b^{-1}/\kappa_s^{-1})^2 \approx 1/3$. This may be explained if the functionalized PMMA spheres acquire their charges by adsorbing cations from solution. The immobilized spheres that are deposited on the walls then prevent these ions from contributing to charge transport. Removing cations from solution in this way would reduce the conductivity of the electrolyte when the volume fraction of spheres is low.

Comparably good results are obtained for pairs of spheres ranging in size from $a_p = 0.55$ μm to $a_p = 2.70$ μm. To more easily compare these measurements, we compute the interparticle potential $U(r)$ by numerically integrating $F(r)$ under the assumption that $\lim_{r\to\infty} U(r) = 0$. Figure 2(e) shows results for 16 pairs of spheres (solid curves) together with statistical uncertainties (shaded regions) and fits to Eq. (13) (dashed curves). To emphasize the agreement between these measurements and theory, we replot representative curves in Fig. 2(f) so that the screened-Coulomb form falls on a line whose slope is κ. For comparison, we also plot the best fit to a pure Coulomb repulsion ($\kappa = 0$) as dashed curves.

How the spheres' charges depend on their radii offers insights into their charging mechanism. The discrete points in Fig. 3 show fit values for $Z^*(a_p)$ plotted as a function of the fit values of κa_p. These results are scaled to emphasize the relationship between effective surface charge and effective surface potential, ζ^*, that is predicted by charge renormalization

theory [3,5,52,53],

$$Z^* \frac{\lambda_B}{a_p} = \left| \frac{e\zeta^*}{k_BT} \right| (1 + \kappa a_p). \qquad (15)$$

The good agreement between our measurements and a one-parameter fit of the data to Eq. (15) for the effective surface
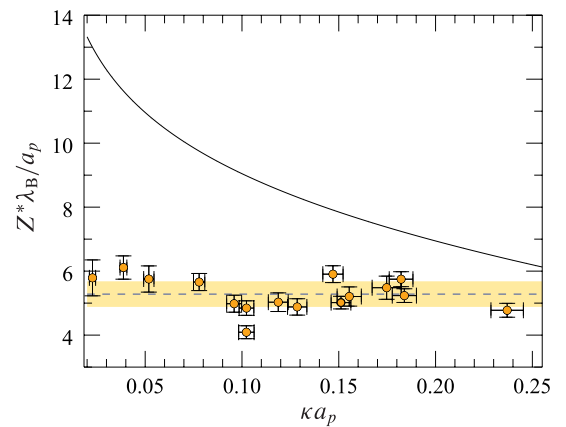

FIG. 3. Effective charge number $Z^*(a_p)$ of PMMA spheres suspended in CXB-odecane with respect to particle size a_p. The solid curve is the limiting effective charge due to counterion condensation from Eq. (16). The dashed horizontal line indicates the mean effective surface potential of $5.2 k_BT$ and the shaded region indicates the uncertainty in this value, $\pm 0.4 k_BT$.

potential, $e\zeta^* = (5.2 \pm 0.4)k_BT$, suggests that the spheres' charges are regulated by a constant surface potential.

The observed linear dependence of Z^* on a_p contrasts with a recent report [15] of complementary measurements on the same system prepared with a higher volume fraction of particles. The quadratic dependence of the effective charge on the particle radius reported in that study is inconsistent with Eq. (15). Having the effective charge be proportional to the surface area could be consistent with charging controlled by the chemical equilibria of weak association and dissociation reactions [54]. Our measurements, by contrast, are consistent with standard thermodynamic mechanisms [4] in a conventional electrolyte, at least for spheres at a very low volume fraction.

The large screening length of the CXB-dodecane mixture creates an additional way to probe the spheres' charging mechanism. According to Poisson-Boltzmann theory [6], the effective charge on a sphere that is small enough to satisfy $\kappa a_p < 1$ is limited by counterion condensation. For spheres dispersed in a 1:1 electrolyte, this limit is [6]

$$Z^* \frac{\lambda_B}{a_p} < 4\ln 2 - 2\ln \kappa a_p + 2\ln(-\ln \kappa a_p)$$

$$-\frac{1}{2}\ln\left(\frac{Z\frac{\lambda_B}{a_p} - 2\ln \kappa a_p}{Z\frac{\lambda_B}{a_p} + 2\ln \kappa a_p}\right) + \mathcal{O}\{1\}, \quad (16)$$

where Z is the sphere's bare charge. This result recently has been shown to be consistent with the measured electrophoretic mobility of highly charged colloidal spheres in low polar solvents under salt-free conditions [55]. Predictions for the present system in the limit of large bare charge are plotted as the solid curve in Fig. 3. The measured values all being well below the Poisson-Boltzmann limit, we conclude that the spheres' effective charges are not reduced by charge renormalization and thus should differ little from the bare charges.

This conclusion is further supported by referring to analytical expressions for to the full Poisson-Boltzmann potential outside a charged sphere [56]. In the domain of the present experiments, $\kappa a_p < 0.3$, $e\zeta^* < 6k_BT$, and $\kappa r \gtrsim 1$, the linearized Poisson-Boltzmann approximation overestimates the potential energy for monovalent ions at distance r from the charged sphere's center by less than 1% [56, see Eq. (8)]. Assuming that the potential energy for a charged sphere centered at the same large separation can be obtained by linear superposition, our fits to experimental estimates for $U(r)$ would thus underestimate the spheres' surface potentials by far

less than the experimental uncertainty. The fit values for the effective charges on the spheres thus should be reasonably good estimates for their bare charges, $Z^* \approx Z$.

Based on these considerations, we propose that the spheres in the present study acquire their charges by association of cations from solution. The presence in solution of protons from the dehydrobromination of CXB suggests a likely source for those cations. With this interpretation, the measured surface potential of $5k_BT$ reasonably corresponds to the energy of association between the cations and the polarizable groups bound to the spheres' surfaces. This potential is below the threshold for charge condensation. Few counterions, therefore, are likely to be associated with the surface. Spheres that are substantially larger than those in the present study might cross over into the regime of strong charge renormalization. Whether that would take the form of cation dissociation or counterion condensation is an open question.

The outstanding puzzle in the present study is that the CXB-dodecane electrolyte appears to be rather conventional. Both conductivity and colloidal interaction measurements suggest the presence of free ions in solution, even though the energetic cost of charge separation should be substantially higher than the thermal energy scale. No organic salt or charge-stabilization agents were added to the solution, nor are any of the system's components likely to form nanoscale structures such as inverse micelles that would allow for stable charge separation at room temperature [57]. The same mechanism that allows for separation of hydrogen and bromide ions in solution is likely to be involved in charging the PMMA spheres. Once they are more fully understood, such organic electrolyte systems will provide interesting model systems with which to study electrostatic coupling in charge-stabilized colloidal dispersions. The high charges and long screening lengths that can be attained will be useful for probing nonlinear screening and the breakdown of pairwise additivity in charged spheres' electrostatic interactions. Understanding and controlling charge transfer mechanisms in simple organic electrolytes such as CXB-dodecane may yield useful alternatives to aqueous electrolytes in practical applications.

[1] W. B. Russel, D. A. Saville, and W. R. Schowalter, *Colloidal Dispersions*, *Cambridge Monographs on Mechanics and Applied Mathematics* (Cambridge University Press, Cambridge, UK, 1989).

[2] J. C. Crocker and D. G. Grier, Phys. Rev. Lett. **73**, 352 (1994).

[3] J. C. Crocker and D. G. Grier, Phys. Rev. Lett. **77**, 1897 (1996).

[4] S. H. Behrens and D. G. Grier, J. Chem. Phys. **115**, 6716 (2001).

[5] S. Alexander, P. M. Chaikin, P. Grant, G. J. Morales, P. Pincus, and D. Hone, J. Chem. Phys. **80**, 5776 (1984).

[6] G. V. Ramanathan, J. Chem. Phys. **88**, 3887 (1988).

[7] L. Antl, J. W. Goodwin, R. D. Hill, R. H. Ottewill, S. M. Owens, S. Papworth, and J. A. Waters, Colloids Surf. **17**, 67 (1986).

[8] C. Pathmamanoharan, K. Groot, and J. Dhont, Colloid Polym. Sci. **275**, 897 (1997).

[9] H. Looyenga, Mol. Phys. **9**, 501 (1965).

[10] M. T. Elsesser and A. D. Hollingsworth, Langmuir **26**, 17989 (2010).

[11] P. N. Pusey and W. van Megen, Nature **320**, 340 (1986).

[12] M. T. Sullivan, K. Zhao, A. D. Hollingsworth, R. H. Austin, W. B. Russel, and P. M. Chaikin, Phys. Rev. Lett. **96**, 015703 (2006).

[13] C. P. Royall, M. E. Leunissen, and A. van Blaaderen, J. Phys.: Condens. Matter **15**, S3581 (2003).

[14] M. E. Leunissen, A. van Blaaderen, A. D. Hollingsworth, M. T. Sullivan, and P. M. Chaikin, Proc. Natl. Acad. Sci. U.S.A. **104**, 2585 (2007).

[15] M. N. van der Linden, J. C. P. Stiefelhagen, G. Heessels-Gürboğa, J. E. S. van der Hoeven, N. A. Elbers, M. Dijkstra, and A. van Blaaderen, Langmuir **31**, 65 (2015).

[16] A. B. Pangborn, M. A. Giardello, R. H. Grubbs, R. K. Rosen, and F. J. Timmers, Organometallics **15**, 1518 (1996).

[17] J. G. Smith, in *Organic Chemistry*, 3rd ed. (McGraw–Hill, New York, 2011), Chap. 8.

[18] R. G. Schmitt, Master's thesis, Worcester Polytechnic Institute (1953).

[19] H. S. Golinkin, D. M. Parbhoo, and R. E. Robertson, Can. J. Chem. **48**, 1296 (1970).

[20] S. M. Hurley, T. E. Dermota, D. P. Hydutsky, and A. W. Castleman, Science **298**, 202 (2002).

[21] S. K. Sainis, J. W. Merrill, and E. R. Dufresne, Langmuir **24**, 13334 (2008).

[22] C. E. Espinosa, Q. Guo, V. Singh, and S. H. Behrens, Langmuir **26**, 16941 (2010).

[23] R. Kemp, R. Sanchez, K. J. Mutch, and P. Bartlett, Langmuir **26**, 6967 (2010).

[24] R. M. Fuoss, J. Am. Chem. Soc. **80**, 5059 (1958).

[25] C. Valeriani, P. J. Camp, J. W. Zwanikken, R. van Roij, and M. Dijkstra, Soft Matter **6**, 2793 (2010).

[26] G. J. Janz and S. S. Danyluk, J. Am. Chem. Soc. **81**, 3854 (1959).

[27] M. N. Sovilj, J. Chem. Eng. Data **40**, 1058 (1995).

[28] R. H. Ottewill, A. R. Rennie, and A. Schofield, in *Trends in Colloid and Interface Science IV. Progress in Colloid & Polymer Science*, edited by M. Zulauf, P. Lindner, and P. Terech, Vol. 81 (Steinkopff, Darmstadt, 1990), pp. 1–5.

[29] C. F. Zukoski, A. P. Gast, D. A. Saville, S. P. Stoylov, B. Vincent, J. Lyklema, P. C. van der Hoeven, P. Bartlett, R. H. Ottewill, A. Schofield, G. Frens, G. Cevc, R. Buscall, N. Ise, M. H. G. M. Penders, J. K. G. Dhont, A. Vrij, W. B. Russel, T. F. Tadors, A. E. Duisterwinkel, and H. J. Ploehm, Faraday Discuss. Chem. Soc. **90**, 57 (1990).

[30] C. P. Smyth, *Dielectric Behavior and Structure* (McGraw–Hill, New York, 1955).

[31] J. Israelachvili, *Intermolecular and Surface Forces*, 3rd ed. (Elsevier, Amsterdam, 2011).

[32] K. E. J. Barrett, *Polymerization in Organic Media* (John Wiley and Sons, London, 1975).

[33] J. C. Crocker and D. G. Grier, J. Colloid Interface Sci. **179**, 298 (1996).

[34] S. K. Sainis, V. Germain, and E. R. Dufresne, Phys. Rev. Lett. **99**, 018303 (2007).

[35] B. W. Silverman, *Density Estimation for Statistics and Data Analysis* (Chapman & Hall, New York, 1992).

[36] E. R. Dufresne and D. G. Grier, Rev. Sci. Instrum. **69**, 1974 (1998).

[37] D. G. Grier, Nature **424**, 810 (2003).

[38] T. Savin and P. S. Doyle, Phys. Rev. E **71**, 041106 (2005).

[39] T. Savin and P. S. Doyle, Biophys. J. **88**, 623 (2005).

[40] M. Polin, D. G. Grier, and Y. Han, Phys. Rev. E **76**, 041406 (2007).

[41] J. Baumgartl and C. Bechinger, Europhys. Lett. **71**, 487 (2005).

[42] A. E. Larsen and D. G. Grier, Nature **385**, 230 (1997).

[43] T. M. Squires and M. P. Brenner, Phys. Rev. Lett. **85**, 4976 (2000).

[44] T. M. Squires, J. Fluid Mech. **443**, 403 (2001).

[45] S. K. Sainis, V. Germain, C. O. Mejean, and E. R. Dufresne, Langmuir **24**, 1160 (2008).

[46] J. W. Merrill, S. K. Sainis, and E. R. Dufresne, Phys. Rev. Lett. **103**, 138301 (2009).

[47] B. J. Krishnatreya, A. Colen-Landy, P. Hasebe, B. A. Bell, J. R. Jones, A. Sunda-Meya, and D. G. Grier, Am. J. Phys. **82**, 23 (2014).

[48] G. K. Batchelor, J. Fluid Mech. **74**, 1 (1976).

[49] J. C. Crocker, J. Chem. Phys. **106**, 2837 (1997).

[50] E. R. Dufresne, T. M. Squires, M. P. Brenner, and D. G. Grier, Phys. Rev. Lett. **85**, 3317 (2000).

[51] I. Rios de Anda, A. Statt, F. Turci, and C. P. Royall, Contrib. Plasma Phys. **55**, 172 (2015).

[52] E. Trizac, L. Bocquet, and M. Aubouy, Phys. Rev. Lett. **89**, 248301 (2002).

[53] E. Trizac, L. Bocquet, M. Aubouy, and H. H. von Grünberg, Langmuir **19**, 4027 (2003).

[54] T. Vissers, A. Imhof, F. Carrique, A. V. Delgado, and A. van Blaaderen, J. Colloid Interface Sci. **361**, 443 (2011).

[55] D. A. J. Gillespie, J. E. Hallett, O. Elujoba, A. F. C. Hamzah, R. M. Richardson, and P. Bartlett, Soft Matter **10**, 566 (2014).

[56] R. Tuinier, J. Colloid Interface Sci. **258**, 45 (2003).

[57] M. F. Hsu, E. R. Dufresne, and D. A. Weitz, Langmuir **21**, 4881 (2005).